Proceedings of the 21st ICSMGE, Vienna, Austria, 14 – 19 June 2026. Pistrol, Adam & Schweiger (eds.)
Published by: ÖGG, Austrian Society for Geomechanics, Salzburg, Austria, ISBN 978-3-9503898-4-5
https://doi.org/10.53243/ICSMGE2026-488

Study of unpaved pavement layers under monotonic loading using scaled models

Phanindra Gudapati, Umashankar Balunaini
Department of Civil Engineering, Indian Institute of Technology Hyderabad, Hyderabad, India, buma@ce.iith.ac.in

ABSTRACT: Model pavement studies are useful in analysing and predicting the behaviour of pavement systems. Despite being uneconomical, large-scale model pavement experiments (LSMPE) offer insights into the behaviour of pavement systems. On the other hand, small-scale model pavement experiments (SSMPE) offer a faster and economical alternative to LSMPE; however, research on SSMPE remain limited. The main objective of this study is to evaluate the response of a scaled pavement model under monotonic loading. Firstly, finite element model is developed in ABAQUS to determine the optimal dimensions of a scaled model. Subsequently, an experimental study is carried out using both large-scale and small-scale models considering circular loading areas of diameters equal to 300 mm and 50 mm, respectively. A large-scale model with dimensions of 1.5m x 1.5m x 1m is used, while the dimensions of the small-scale model are scaled down relative to the size of the loaded area. The subgrade consisted of clayey sand with a California bearing ratio (CBR) equal to 5%. Two sections are considered in the study: a) subgrade soil alone, and b) an aggregate layer overlying subgrade soil. Tests are conducted on both unreinforced and geogrid reinforced sections in both large- and small- scale models. The benefit ratios of reinforced beds obtained from both models are compared for different settlement ratios of the loading plate. Results showed that the unreinforced cases exhibited good agreement between the two models, while the reinforced cases showed a variation in the range of 5–15%, particularly when geogrid is embedded within the aggregate layer overlying subgrade soil. Based on these findings of the study, the limitations associated with developing scaled model are discussed. The study concludes that the proposed small-scale model is simple to use for pavement testing and provides results in a reasonably quick time.

KEYWORDS: Large-scale model, small-scale model, unpaved pavement layers, monotonic loading, geogrid reinforcement.

1 INTRODUCTION

With rapid urbanization and economic development, the demand for transportation infrastructure has significantly increased. India currently has the second-largest road network in the world of about 6.2 million kilometers, with a growing emphasis on the development of national highways designed to accommodate heavy traffic loads (MoRTH, 2025).

A conventional flexible pavement system typically consists of a subgrade, subbase, base, and bituminous layers. For high-traffic categories, the thickness of each layer is increased to enhance structural capacity and durability. However, this results in higher construction costs and increased material consumption (Goud et al. 2020). Therefore, there is a growing need to adopt alternative solutions that can improve pavement performance while maintaining cost-effectiveness and construction efficiency. One such proven solution is the use of geosynthetics, which have gained widespread application in pavements over the past few decades. Geosynthetics are known to enhance load distribution, reduce rutting, and improve the stability of pavement layers (Giroud et al. 1984; Ahmed Kamel et al. 2004; Abu-Farasakh et al. 2016). Their use in subgrade stabilization (Baadiga & Balunaini 2024) and reinforcement in base/subbase layers has been shown to reduce required thicknesses and improve service life without compromising performance (Al-Qadi et al. 1994; Abu-Farasakh et al. 2016). Design guidelines for use of geogrid in flexible pavements are provided by Indian Roads Congress, IRC: SP: 59 (2019) and the incorporation of geosynthetics in pavement design is further supported in IRC-37 (2018).

To investigate the mechanical response of flexible pavement sections, several researchers have conducted large-scale model tests using various test tank sizes, typically ranging from 0.9 m x 0.9 m x 0.6 m to 2.2 m x 2.2 m x 1.7 m (length x width x height) (Perkins, 1999; Chen et al. 2009; Goud et al. 2022, etc.). While such large-scale tests provide realistic insights into pavement behavior, they require substantial quantities of material, and are labor-intensive and time-consuming. To address these limitations, the use of small-scale models presents a practical alternative. When properly scaled, small-scale studies can effectively replicate large-scale pavement responses and offer a more efficient and economical approach for evaluating pavement performance.

Despite extensive research and field implementation, the quantification of performance in terms of modulus enhancement due to geosynthetic inclusion, remains a critical area of interest. This study focuses on the evaluation of improvement of geogrid-reinforced aggregate layer using both large-scale and scaled model tests, offering insights into behaviour of scaled models. In addition to assessing the improvement from geogrid reinforcement, this study investigates the viability of using scaled models as a reliable tool for replicating large-scale pavement behaviour. The findings provide valuable insights from small-scale model experimentation on geosynthetic performance in unpaved pavement systems and draws conclusions through comparison of small-scale models with large-scale models.

2 MATERIALS

2.1 *Subgrade soil*

Locally available soil was selected as the subgrade material. Figure 1 shows the grain-size distribution of the subgrade soil from wet sieve and hydrometer analysis. The liquid limit, plastic limit, and plasticity index were found to be 38.2%, 20.6%, and 17.6% respectively. According to the Unified soil classification system (USCS), the soil is classified as clayey sand (SC). The specific gravity of the soil is 2.62 and differential free swell index was measured to be approximately 15%, indicating low swelling potential. Proctor compaction tests, conducted in accordance with ASTM D698 (2021), yielded the maximum dry density (MDD) of 20.2 kN/m^3 and optimum moisture content (OMC) of 9.2%. To achieve a CBR of 5%, several CBR tests were carried out on samples with different compacted densities and moisture contents, in accordance with ASTM D1883 (2021). The target CBR of 5% was achieved at a dry density of 18.7 kN/m^3 and moisture content of 13.5%.

2.2 *Aggregate material*

A locally procured quarry aggregate material was used as a base and subbase layers. The material satisfies the gradation requirements specified by the Ministry of Road Transport and

Highways, MoRTH (2013). Figure 1 presents the grain-size distribution of the aggregate material. The maximum dry density and the optimum moisture content of the aggregate material were determined to be 21.87 kN/m^3 and 6.6%, respectively.

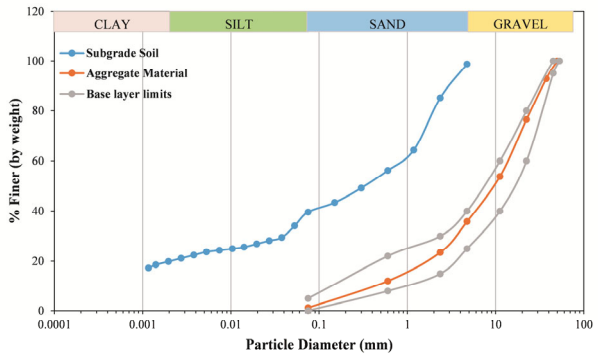

Figure 1. Grain-size distributions of subgrade soil and aggregate material.

2.3 *Geogrids*

Two types of geogrids were used as reinforcement materials in the study. The ultimate tensile strengths of the two grids were equal to 30 x 30 kN/m and 60 x 60 kN/m in both machine and cross machine directions. Figure 2 presents the photographs of geogrids used, while Table 1 summarizes the properties of the geogrids.

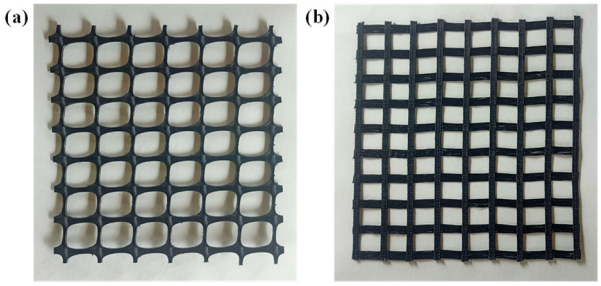

Figure 2. Geosynthetics used in the study (a) PP30 (b) PET60.

Table 1. Properties of geogrids obtained from the manufacturer.

Particulars	Geogrid 1	Geogrid 2
Polymer	Polypropylene (PP)	Polyethylene Terephthalate (PET)
Geogrid type	Biaxial	Biaxial
Aperture size in MD x CMD[a] (mm)	38 x 38	25 x 20
Ultimate tensile strengths in MD and CMD (kN/m)	30 x 30	60 x 60

[a] MD: Machine direction, and CMD: Cross machine direction.

3 METHODOLOGY OF THE STUDY

The present study aims to establish a correlation between the large-scale and small-scale pavement models. In this study, scaling was applied to the model dimensions while keeping the material properties constant.

The study involves both numerical simulations and experimental investigations of both the models. Firstly, numerical modelling was taken up, followed by experimental testing. The results from various small-scale models were compared with large-scale model to identify a suitable small-scale model configuration for experimental validation. Once the appropriate small-scale and large-scale models were finalized, corresponding experiments were conducted on both models and their results are compared. Figure 3 gives the complete workflow of the study.

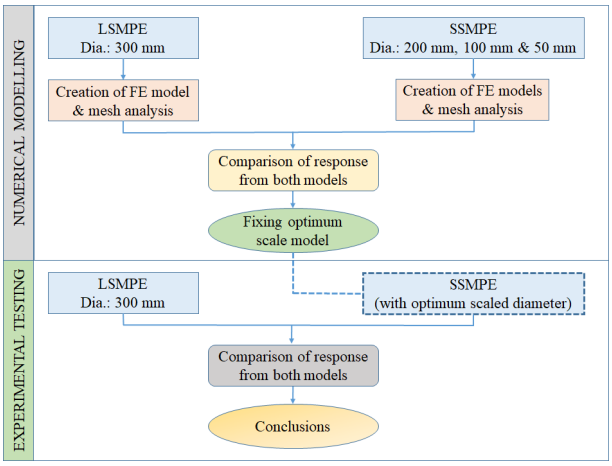

Figure 3. Flowchart showing the methodology of the study.

4 FINITE ELEMENT ANALYSIS

4.1 *Description of models*

For finite element analysis, the dimensions of the LSMPE were first determined. A circular plate with a diameter equal to 300mm was used to replicate the actual wheel contact area. The depth and width of the large-scale model were considered as 3B and 5B, i.e., 900mm and 1500mm, respectively (where B is diameter of the loading plate), to minimize boundary effects. (refer to Figure 4 (a)).

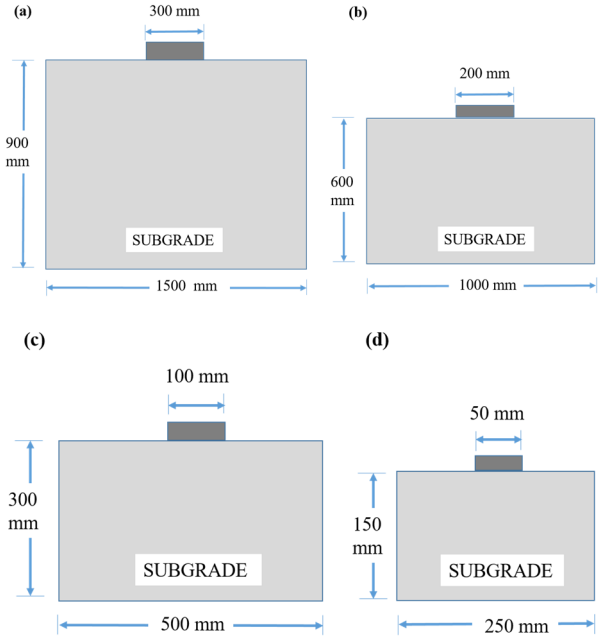

Figure 4. Model test dimensions of (a) LSMPE (b) SSMPE-Case1 (c) SSMPE-Case2 (d) SSMPE-Case3.

For SSMPE, three different cases using the loading plates with diameters of 200mm, 100mm and 50mm were considered. In the scaling process, the plate diameter was considered as the key parameter, as the loading area plays a significant role in the elastic analysis. The dimensions of the small-scale models were scaled with respect to the diameter of the large-scale model to maintain geometric similarity. The model configurations for the three small-scale cases are presented in Figure 4(b), (c) & (d).

4.2 *Numerical modelling*

For the finite element analysis, ABAQUS was used. An axisymmetric model was considered for both large-scale and all small-scale models. For LSMPE, a circular loading area of radius of 150mm was considered, applied on a homogenous soil medium of depth of 900mm and width 750mm. Similar to LSMPE, same homogenous soil medium is considered in SSMPE and the scaled down geometry of small-scale models were defined as follows:

- SSMPE Case 1: Radius of loading area = 100mm, soil depth = 600mm, width = 500mm.
- SSMPE Case 2: Radius of loading area = 50mm, soil depth = 300mm, width = 250mm.
- SSMPE Case 3: Radius of loading area = 25mm, soil depth = 150mm, width = 125mm.

A uniform pressure of 100 kPa was applied over the respective plate radius in all models. The boundary conditions were kept consistent across all models. At the bottom edge, movement was restricted in both vertical and horizontal directions. On the sides, the axisymmetric boundary condition was applied on one side, while on the other side, movement was allowed in vertical direction only. For all models, the subgrade was modelled using an extended Drucker-Prager constitutive model with hyperbolic yielding criterion. The material properties for subgrade were sourced from the Leng & Gabr (2005) and are summarized in Table 2.

Table 2. Properties of material used in modelling (sourced from Leng et al. 2005).

Parameters	Values
Material	Subgrade
Model and parameters	Drucker-Pager and $\beta=10^0$, $P_{t|0}=10$ kPa , $\psi=0^0$
Yielding stress (kPa)	43.6
Young's modulus *E* (MPa)	10
Poisson's ratio *v*	0.42

The element type CAX4R was used for all the models and the mesh convergence analysis was performed and the results are presented in Table 3.

Table 3. Mesh analysis of the models.

S. No	No. of Elements	Maximum Deformation (mm) LSMPE	SSMPE Case 1	SSMPE Case 2	SSMPE Case 3
1	90	2.144	1.429	0.714	0.357
2	270	2.129	1.419	0.709	0.354
3	360	2.129	1.419	0.709	0.354

The mesh convergence study commenced with 90 elements per model and was refined further to 270 and 360 elements. The convergence study was conducted by comparing the maximum deformation for the different mesh sizing. The results were found to converge for 270 elements and higher, with negligible variation in the maximum deformation beyond this point. Accordingly, a mesh size corresponding to 270 elements was adopted for all subsequent analyses to ensure a balance between computational efficiency and the accuracy in the results.

4.3 *Validation and results*

The numerical analysis results were used to evaluate the stress distribution under the applied loading. The stress distribution along the depth for LSMPE model was compared with Boussinesq's solution, as shown in Figure 5(a). Similarly, the stress distribution for each SSMPE case was compared with Boussinesq's solution and is presented in Figure 5(b). From Figure 5(a) & 5(b), it was observed that the numerical results show a good agreement with Boussinesq's solution, thereby validating the accuracy of both large-scale and small-scale models.

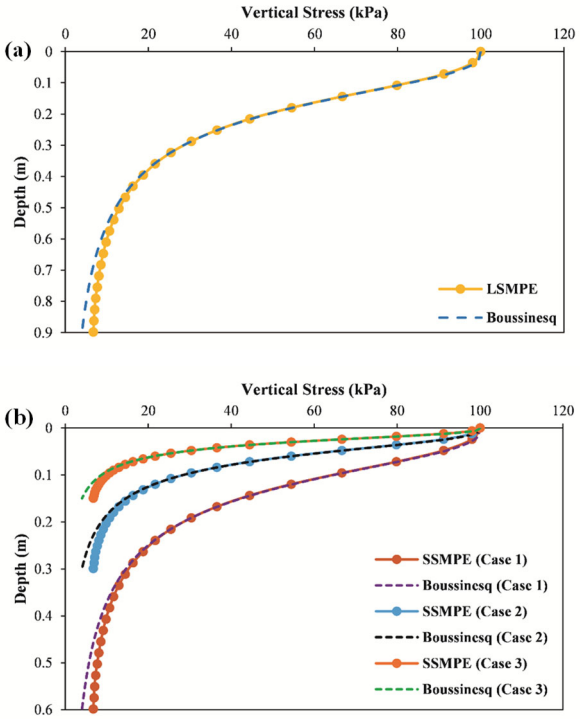

Figure 5. Comparison of vertical stresses with depth from FE model and elastic solution considering (a) large-scale model geometry (b) small-scale model geometries (Cases 1, 2, 3).

From both set of results, it was observed that the models show good match with Boussinesq's solution up to the depth of approximately 1.5-2B (where B is the respective plate diameter). Beyond this depth, the finite element model predicts slightly higher stress values compared to Boussinessq's solution. This discrepancy arises because Boussinessq's theory assumes a semi-infinite medium, whereas the models used in the present study have a finite thickness. Similar observations have been reported by Leng & Gabr (2005) and Keskin et al. (2023).

For comparison between the models, the vertical stress obtained at different depths was analyzed. The vertical stress developed at the depths of 0.5B, 1B, 1.5B, 2B, 2.5B (where B is diameter of the plate) of LSMPE model were compared with those of each SSMPE case, are presented in Table 4.

Table 4. Comparison of vertical stress values for different normalized depths between LSMPE and SSMPE-Cases 1, 2, 3.

S.No	Depth, z	Vertical stress (kPa) LSMPE	SSMPE Case 1	SSMPE Case 2	SSMPE Case 3
1	0.5B	66.51	64.51	64.51	64.51
2	1B	28.61	28.61	28.61	28.61
3	1.5B	15.31	15.31	15.31	15.31
4	2B	10.05	10.05	10.05	10.05
5	2.5B	7.73	7.73	7.73	7.73

The results show that the vertical stress decreases with increasing depth across all the models, which aligns with findings reported by Keskin et al. (2023). Furthermore, the vertical stress values obtained from each SSMPE case closely

match those from the LSMPE model, indicating the high level of agreement and validating the effectiveness of the scaled models.

A finite element analysis was conducted to evaluate the load-settlement behavior of the models under static loading. A uniform pressure of 100 kPa was applied in all cases. The resulting pressure versus settlement responses were analyzed and are presented in Figure 6. The results indicate that, under the same applied pressure and material properties, the LSMPE model exhibits higher settlement compared to the SSMPE cases. Among the SSMPE models, settlement decreases as the plate diameter reduces, demonstrating a clear influence of scale on the deformation response.

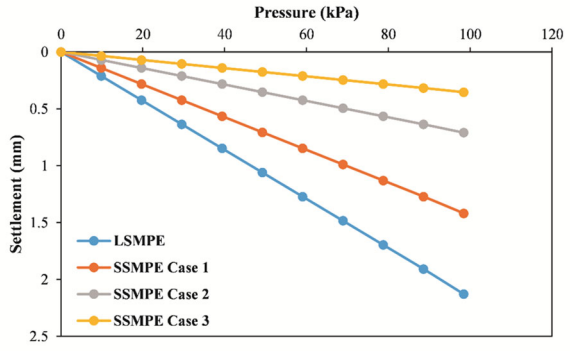

Figure 6. Pressure vs. settlement plots for LSMPE & SSMPE considering Cases 1, 2, 3.

For comparison among the models, the settlements are normalized with respect to the diameter of the loading plate used in each respective model. Table 5 gives the comparison for each SSMPE case. The results indicate that the pressure obtained to the corresponding normalized settlement of all SSMPE cases exactly matches with those of the LSMPE model, confirming the validity of the scaling approach.

Table 5. Comparison of pressures for different given settlement ratios between the models.

S.No	s/B (%)	Pressure (kPa)			
		LSMPE	SSMPE Case 1	SSMPE Case 2	SSMPE Case 3
1	0.2	27.85	27.85	27.85	27.85
2	0.4	55.70	55.70	55.70	55.70
3	0.6	83.56	83.56	83.56	83.56

4.4 *Fixing optimal scaled model*

From the FEM analysis of both the LSMPE and SSMPE considering the three cases of this study, it is evident that the large-scale pavement response can be effectively simulated using scaled models. As reported in the Table 5, the pressure values corresponding to different normalized settlements for both the large-scale and small-scale models are found to closely match, indicating consistent deformation behavior. Furthermore, Table 4 demonstrates that the vertical stresses at normalized depths in the LSMPE model align well with those observed in the SSMPE cases. This consistency confirms that the stress distribution is similar in both large and scaled models, validating the reliability of the scaled modeling approach for replicating full-scale pavement behavior.

Based on this understanding, all the three scaled models were found to be effective in reproducing the large-scale behaviour. However, considering cost and time efficiency in sample preparation, the authors selected the smallest plate diameter of 50mm for further experimental validation. Accordingly, the model dimensions of 250 mm in width and 150 mm in depth were adopted for subsequent testing.

5 EXPERIMENTAL PROGRAM

This study comprised of both large-scale and small-scale experimental tests under monotonic loading. The large-scale tests were conducted in a test tank with dimensions of 1.5 m × 1.5 m × 1 m. A circular steel plate with a diameter of 300 mm was used for load application. A 100 kN capacity actuator, equipped with inbuilt load and displacement sensors, was employed to apply the load. For the small-scale tests, a 50 mm diameter loading plate was used in a cylindrical test tank measuring 250 mm in diameter and 167 mm in depth. A 50 kN capacity load cell and a Linear Variable Differential Transformer (LVDT) with a range of 25mm were used to measure load and displacement, respectively. The loading rate for large-scale model experiments was maintained as 0.5 mm/min, while rate for the small-scale tests was proportionally scaled relative to the plate diameter, resulting in a loading rate of 0.083 mm/min.

In both experimental setups, testing commenced with the subgrade alone in an unreinforced condition, followed by tests incorporating geogrid reinforcement. Additionally, tests were then conducted with an aggregate layer placed over the subgrade under both unreinforced and reinforced configurations. The detailed testing procedures and corresponding results are presented in the following sections.

5.1 *Subgrade soil alone*

For the LSMPE model, a subgrade thickness of 900 mm was adopted. The subgrade material was prepared by adding the required amount of water to achieve the target moisture content, followed by thorough mixing to ensure uniformity. The soil was then compacted in 100 mm thick layers, targeting a CBR of 5%. To verify the compaction quality and uniformity, Dynamic Cone Penetration (DCP) tests were conducted on each compacted layer at different locations. The results confirmed that the target CBR of 5% was consistently achieved, with a variability of ±0.5% across the layers.

For the SSMPE model, a subgrade thickness of 150 mm was used. The preparation process is similar to that of LSMPE model, with the soil thoroughly mixed at the required moisture content and compacted in scaled layer thicknesses appropriate to the reduced model dimensions. A target CBR of 5% is achieved.

Following sample preparation, both models are subjected to loading the subgrade section. The pressure-settlement response for both LSMPE and SSMPE are presented in Figure 7(a). It is understood that, for the same applied pressure, LSMPE model exhibited greater settlement than the SSMPE model, a trend consistent with the numerical predictions shown in Figure 6.

To enable a comparative assessment, pressure versus normalized settlement (settlement with respect to the respective plate diameter) was plotted, as shown in Figure 7(b). The results reveal that the SSMPE model closely replicates the response of the LSMPE model. Across different normalized settlement values, the variation in pressure between the two models is in the range of ±5%. This minimal difference validates the effectiveness of the scaled approach in simulating the large-scale behavior of unreinforced pavement sections under monotonic loading.

For the reinforced subgrade section, PP30 geogrid was used in both the models. In the LSMPE model, the geogrid was positioned at a depth of 100 mm below the loading plate, consistent with the placement reported by Duddu et al. (2024).

To maintain geometric similarity, the reinforcement in the SSMPE model was placed at the same z/B ratio of 0.33. Monotonic load tests were conducted and resulting pressure-normalized settlement plots are shown in Figure 8.

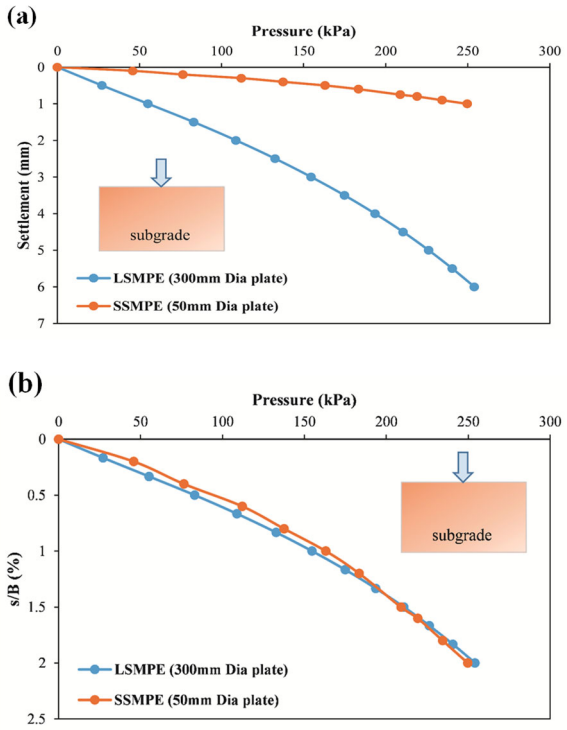

Figure 7. Comparison of behavior of subgrade from LSMPE and SSMPE presented in the form of (a) pressure vs. settlement plot (b) pressure vs. normalised settlement.

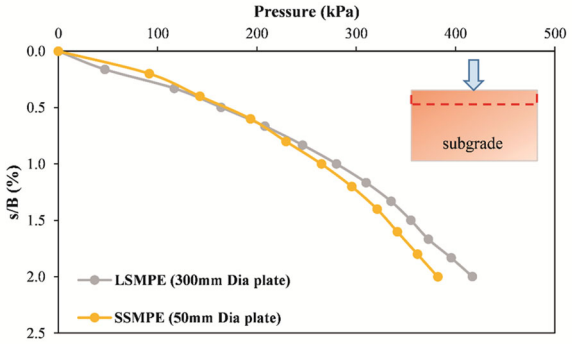

Figure 8. Comparison of pressure vs. normalised settlement of reinforced subgrade from LSMPE and SSMPE testing.

The results indicate that both LSMPE and SSMPE models exhibit significantly improved performance compared to the unreinforced section presented in Figure 7, aligning with findings from previous studies (Mandel & Sah, 1992; Ahmed Kamel et al. 2004; Duddu et al. 2024). At a normalized settlement of 2%, both unreinforced models sustained a pressure of approximately 250 kPa. However, under reinforced conditions, the pressure-carrying capacity increased to nearly 400 kPa, highlighting the effectiveness of geogrid reinforcement in enhancing load-carrying capacity and reducing deformations in subgrade layers. The SSMPE model demonstrated a response closely aligned with that of the LSMPE model. Although deviations in the range of 10% were noted beyond the pressure level of 250 kPa, the overall agreement affirms the reliability of the small-scale model in replicating the reinforcement behavior observed in large-scale tests.

5.2 *An aggregate layer overlying subgrade soil*

To evaluate the performance of the scaled model in simulating unpaved pavement section, an aggregate layer (combined base/sub-base layer) was placed over a subgrade with a target CBR 5% in both large-scale and small-scale models. For the LSMPE configuration, the total depth was 940 mm, consisting of 500 mm of subgrade and 440 mm of aggregate layer. In the SSMPE model, z/B ratios with respect to each layer were maintained same as LSMPE. All dimensions were maintained within a tolerance of ±0.2 mm to ensure geometric similarity with the large-scale model. The subgrade in both models was prepared using the same procedure as in the previous tests, while the aggregate layer was compacted to its OMC and MDD. The responses for both models are presented in Figure 9.

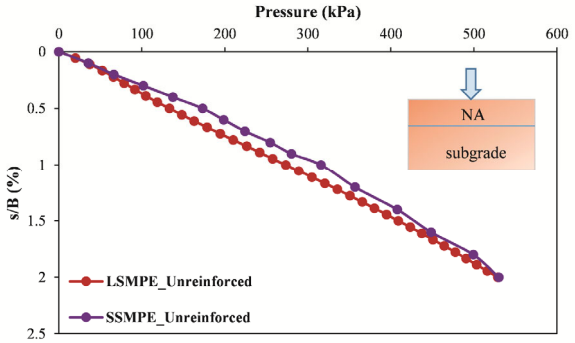

Figure 9. Comparison of pressure vs. normalised settlement of granular layer overlying subgrade from LSMPE and SSMPE testing.

To investigate the reinforced configuration, PET60 geogrid was used as reinforcement and was placed at a depth of one-third of the thickness of the aggregate layer in both models, consistent with previous studies (Goud et al. 2020; Abu-Farsakh et al. 2016). Experimental tests were carried out on reinforced configurations, and the results are presented in Figure 10.

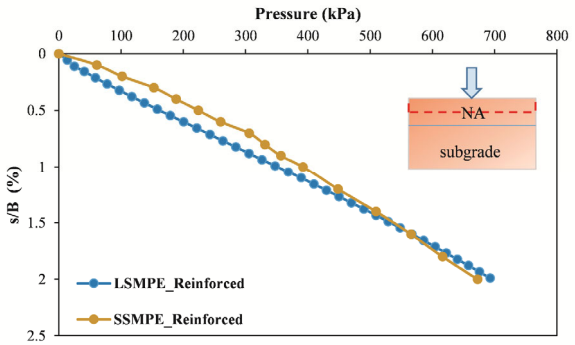

Figure 10. Comparison of pressure vs. normalized settlement of reinforced granular layer overlying subgrade from LSMPE and SSMPE testing.

Both models followed a similar response trend; the reinforced section exhibits improvement than unreinforced section, consistent with findings (Al-Qadi et al. 1994; Chen et al. 2009; Saride et al. 2022). The SSMPE model exhibited slightly higher pressure values at comparable settlements, variations were observed to be within the range of 5-15% in both unreinforced and reinforced sections.

The improvement ratios for the subgrade tests and the tests on aggregate overlying subgrade were analyzed for both LSMPE and SSMPE models. Table 6 gives the improvement ratios evaluated at different settlement-to-width ratios. For reinforcement in subgrade soil alone, the improvement ratios for the s/B ratios of 1, 1.5, 2% was varies from 1.64 to 1.80 for

LSMPE and from 1.53 to 1.62 for SSMPE. In case of the reinforced aggregate layer overlying subgrade, improvement ratios for the s/B ratios of 1, 1.5, 2% was varies 1.28 to 1.32 for LSMPE and from 1.24 to 1.27 for SSMPE. These results indicate a close agreement between the two models, with the improvement ratios demonstrating consistent trends, thereby reinforcing the validity of the scaled model in replicating the performance enhancements observed in large-scale tests.

Table 6. Comparison of improvement ratios between both models.

S.No		SUB-PP30		SUB-AGG-PET60	
	s/B (%)	LSMPE	SSMPE	LSMPE	SSMPE
1	1.0	1.80	1.62	1.28	1.24
2	1.5	1.69	1.59	1.30	1.26
3	2.0	1.64	1.53	1.32	1.27

6 CONCLUSIONS

This study involved both numerical and experimental investigations on load-settlement behavior of unpaved pavement layers under monotonic loading considering large-scale and small-scale models. A comparison is clearly drawn from the different sized model studies. Based on the findings, the following conclusions can be drawn:

- Numerical results indicate that the variation of vertical stress and pressure-settlement responses expressed with normalized settlements from LSMPE and SSMPE models (scaled with respect to plate diameter of 200mm, 100mm and 50mm) are in close agreement.
- Experimental results show that small-scale model studies with loading via a 50 mm diameter plate effectively replicates the response of the unreinforced subgrade condition more accurately than in the case aggregate overlying subgrade configurations.
- The variations in load-settlement response between the large-scale and small-scale models was less than 10% for subgrade alone case, and within 5-15% for aggregate over subgrade conditions.

These findings validate the use of scaled model as a practical approach for assessing the performance of geogrid-reinforced pavement systems. The proposed small-scale model offers a simplified, cost-effective, and time-efficient method for simulating pavement behaviour under controlled conditions. However, this study is limited to the use of planar reinforcement only. To achieve a better agreement in scaled models involving aggregate layers overlying subgrade soil, future research may consider adopting a scaled model with a slightly larger plate diameter to further refine the correlation with large-scale behavior.

7 ACKNOWLEDGEMENTS

The authors declare that no external support was received in the conduct of this study.

8 REFERENCES

Abu-Farsakh, M.Y., Akond, I. and Chen, Q., 2016. Evaluating the performance of geosynthetic-reinforced unpaved roads using plate load tests. *International Journal of Pavement Engineering*, *17*(10), pp.901-912.

Ahmed Kamel, M., Chandra, S. and Kumar, P., 2004. Behaviour of subgrade soil reinforced with geogrid. *International Journal of Pavement Engineering*, *5*(4), pp.201-209.

Al-Qadi, I.L., Brandon, T.L., Valentine, R.J., Lacina, B.A. and Smith, T.E., 1994. Laboratory evaluation of geosynthetic-reinforced pavement sections. *Transportation research record*, (1439), pp.25-31.

ASTM D1883, 2021. Standard test method for California Bearing Ratio (CBR) of laboratory-compacted soils, *ASTM International*, West Conshohocken, PA. https://doi.org/10.1520/D1883-21

ASTM D698, 2021. Standard test methods for laboratory compaction characteristics of soil using standard effort (12,400 ft-lbf/ft^3 (600 kN-m/m3)). *ASTM International*, West Conshohocken. https://doi.org/10.1520/D0698-12R21

Baadiga, R. and Balunaini, U., 2024. Effective CBR and elastic modulus of geogrid-stabilized prepared subgrades overlying existing soft subgrades. *International Journal of Geosynthetics and Ground Engineering*, *10*(3), p.41.

Chen, Q., Abu-Farsakh, M. and Tao, M., 2009. Laboratory evaluation of geogrid base reinforcement and corresponding instrumentation program. *Geotechnical testing journal*, *32*(6), pp.516-525.

Duddu, S.R., Kommanamanchi, V., Chennarapu, H. and Balunaini, U., 2024. Field evaluation of deformation modulus of geogrid and geocell-stabilized subgrade soil. *KSCE Journal of Civil Engineering*, *28*(11), pp.4944-4960.

Giroud, J.P., Ah-Line, C. and Bonaparte, R., 1984. Design of unpaved roads and trafficked areas with geogrids. In *Polymer grid reinforcement* (pp. 116-127). Thomas Telford Publishing.

Goud, G.N., Mouli, S.S., Umashankar, B., Sireesh, S. and Madhira, R.M., 2020. Design and sustainability aspects of geogrid-reinforced flexible pavements—An Indian perspective. *Frontiers in Built Environment*, *6*, p.71.

Goud, G.N., Ramu, B., Umashankar, B., Sireesh, S. and Madhav, M.R., 2022. Evaluation of layer coefficient ratios for geogrid-reinforced bases of flexible pavements. *Road materials and pavement design*, *23*(1), pp.199-210.

IRC, S., 2019. 59: Guidelines for use of geosynthetics in road pavements and associated works. In *The Indian Road Congress, New Delhi*.

IRC, 2018. 37: Guidelines for the design of flexible pavements (4th Revision). *Indian Road Congress*, New Delhi, India.

Keskin, M.S., Bildik, S. and Laman, M., 2023. Experimental and numerical studies of vertical stresses beneath the circular footings on sand. *Applied Sciences*, *13*(3), p.1635.

Leng, J. and Gabr, M.A., 2005. Numerical analysis of stress–deformation response in reinforced unpaved road sections. *Geosynthetics International*, *12*(2), pp.111-119.

Mandal, J.N. and Sah, H.S., 1992. Bearing capacity tests on geogrid-reinforced clay. *Geotextiles and Geomembranes*, *11*(3), pp.327-333.

MoRTH, 2013. (Ministry of Road Transport and Highways). *Specifications for road and bridge works*. New Delhi, India: MoRTH.

MoRTH, 2025. Basic road statistics of India (2019–2020). Ministry of Road Transport and Highways [Online] Available at : https://morth.nic.in/sites/default/files/Basic%20Road%20Statistics%20of%20India-2019-20.pdf [Accessed 10th July 2025].

Perkins, S.W., 1999. Mechanical response of geosynthetic-reinforced flexible pavements. *Geosynthetics international*, *6*(5), pp.347-382.

Saride, S., Baadiga, R., Balunaini, U. and Madhira, M.R., 2022. Modulus improvement factor-based design coefficients for geogrid-and geocell-reinforced bases. *Journal of Transportation Engineering, Part B: Pavements*, *148*(3), p.04022037.